Visual Axis and Stiles–Crawford Effect Peak Show a Positional Correlation in Normal Eyes: A Cohort Study

Seung Pil Bang,[1] Jiakai Lyu,[2] Cherlyn J. Ng,[3] and Geunyoung Yoon[3]

[1]Department of Biomedical Engineering, University of Rochester, Rochester, New York, USA
[2]Institute of Optics, University of Rochester, Rochester, New York, USA
[3]College of Optometry, University of Houston, Houston, Texas, USA

Correspondence: Geunyoung Yoon, College of Optometry, University of Houston, 4901 Calhoun Road, Houston, TX 77204, USA; gyoon2@central.uh.edu.

PURPOSE. The purpose of this study was to locate the visual axis and evaluate its correlation with the Stiles–Crawford effect (SCE) peak.

METHODS. Ten young, healthy individuals (20 eyes) were enrolled. An optical system was developed to locate the visual axis and measure SCE. To locate the visual axis, 2 small laser spots at 450 nm and 680 nm were co-aligned and delivered to the retina. The participants were asked to move a translatable pinhole until these spots were perceived to overlap each other. The same system assessed SCE at 680 nm using a bipartite, 2-channel (reference and test) Maxwellian-view optical system. The peak positions were estimated using a two-dimensional Gaussian fitting function and correlated with the visual axis positions.

RESULTS. Both the visual axis (x = 0.24 ± 0.35 mm, y = −0.16 ± 0.34 mm) and the SCE peak (x = 0.27 ± 0.35 mm, y = −0.15 ± 0.31 mm) showed intersubject variability among the cohort. The SCE peak positions were highly correlated in both the horizontal and vertical meridians to the visual axes (R^2 = 0.98 and 0.96 for the x and y coordinates, respectively). Nine of the 10 participants demonstrated mirror symmetry for the coordinates of the visual axis and the SCE peak between the eyes (R^2 = 0.71 for the visual axis and 0.76 for the SCE peak).

CONCLUSIONS. The visual axis and SCE peak locations varied among the participants; however, they were highly correlated with each other for each individual. These findings suggest a potential mechanism underlying the foveal cone photoreceptor alignment.

In cataract/corneal refractive surgery, accurate centration of optical correction is imperative to obtain optimal visual outcomes. Nevertheless, locating the correction center has been a highly controversial topic.[1] One of the commonly used references for centration is the entrance pupil center (EPC), wherein the optical axis of the instrument is along the line of sight (LOS). Alternatively, the coaxially sighted corneal light reflex (CSCLR), which is a practicable centration reference proximate to the corneal intercept of the visual axis, has also been introduced.[2] The CSCLR is the first Purkinje image observed by the examiner along the identical path with a light source, such that it falls on the line from the fixation point to the center of the anterior corneal curvature.[3] Clinically, the CSCLR-centered correction was reported to be superior to the EPC-centered correction regarding lower induction of total higher-order aberrations.[4–6] Chang et al.[7] showed that centration locations deviated from the EPC to the CSLCR about 80% to 100% were reliable for myopic laser in situ keratomileuses.

Based on the results from recent clinical studies, the visual axis may be a logical candidate for the preferred reference axis, especially for centration, because the visual axis serves as the actual path that a person views.[2,8] However, identifying the visual axis is difficult in a clinical setting because nodal points, which are the cardinal points in optics, have no corresponding anatomic landmarks. Ivanoff[9] first introduced the concept of the foveal achromatic axis, and Thibos et al.[10] interpreted Ivanoff's concept as a functional definition of the visual axis. They proposed that a pinhole should be situated on the pupillary intersection of the visual axis to minimize the effect of transverse chromatic aberration (TCA), and the pinhole is on the achromatizing pupil position as the achromatic axis becomes the visual axis. However, locating the visual axis has been challenging, particularly in a clinical setting.

The human eye has a unique directional sensitivity (i.e. the Stiles–Crawford effect [SCE]).[11] It is a phenomenon that a light beam transmitted through the peripheral region of the pupil is not perceived to be as bright as that through the EPC.[11] Generally, the cone photoreceptors serve as optical fibers that capture light more effectively when illuminated along their axes and tend to point toward the same position on the pupil plane.[12–15] However, a waveguide model of the photoreceptors cannot explain the possibility of inter-receptor crosstalk (i.e. light leakage and re-capture by adjacent photoreceptors). Vohnsen et al.[16] suggested that the volumetric intersection model, based on light absorption by visual pigments in the elongated, layered outer segment of the cone photoreceptor, could explain this gap in understanding.[17,18] However, this model cannot support the

Investigative Ophthalmology & Visual Science

phototropism.[19–24] The pupil coordinates of the peak sensitivity may demonstrate the pupillary location at which the cones aim. In a study population, cones showed a tendency to be directed slightly nasal to the EPC,[25] but large intersubject variability and SCE peak sensitivity pupil positions farther than 1 mm from the EPC have also been reported.[19] It is still controversial which mechanism stimulates the cones to aim at a specific pupil position, and the mechanism is probably related to the visual axis in that both the visual axis and SCE peak remarkably deviate from the EPC. This study aimed to evaluate whether the visual axis is correlated with the SCE peak position on the pupil plane compared to the CSCLR and EPC. We developed a custom-built optical system to measure the positions of the visual axis, SCE peak, CSCLR, and EPC.

METHODS

Ethics Statements

The tenets of the Declaration of Helsinki were observed, and the protocol was approved by the Institutional Review Board of the University of Houston (approval number: 00003196). Written informed consent was obtained from all participants.

Apparatus

An optical system was designed to investigate the achromatizing pupil (visual axis) position and SCE peak position with a common optical path. Figure 1 shows a configuration of the optical system. In the common path, the participant's pupil was optically conjugated with a pinhole (PH1, 600 μm diameter) using a 4-f system relayed with lenses L1

and L2 (both 100 mm focal length, achromatic doublets). Real-time sequential images of the participant's pupil superimposed by the pinhole were recorded using a pupil camera (DCC1545M; Thorlabs). A reticle was located at the pupil plane in front of the M1 and was used to ensure the participant's pupil centration. The pupil camera captured images of the participant's pupil, pinhole position, and reticle at the same time. For pupil alignment, the eye was illuminated with a 4 cm diameter circular array of infrared light-emitting diodes (LEDs; central $\lambda = 870$ nm) located 6 cm from the participant's pupil plane. Chin and forehead rests were used to stabilize the participant's head.

In the assessment of the visual axis, the visual stimuli consisted of two monochromatic (red and blue) sources to generate the chromatic visual test: a red super-luminescent diode (SLD; $\lambda = 680 \pm 3.5$ nm) with a collimating lens (30 mm focal length, achromatic doublet) and a blue laser diode ($\lambda = 450$ nm) with the same collimating lens. Two synchronized rotating choppers were used to create two anti-phase flickering stimuli at 2 hertz (Hz). Neutral density filters were applied to optimize the brightness of the two stimuli. A beam splitter (BS4) and a mirror (M2) were used to direct the two chromatic sources coaxially to the optical path toward the eye. The pinhole (600 μm diameter) on the pupil plane was motorized and translatable in the horizontal and vertical directions so participants could easily adjust the pinhole position using two controllers.

In assessing the SCE, the first light source was a digital micromirror device (DMD; DLP Discovery 4100 0.7XGA; Texas Instruments) relayed by lens L4 and a flipping mirror (M3). A bandpass filter with a 10-nm bandwidth centered at a wavelength of 680 nm was applied in front of L4. The DMD provided the participant with a 0.9 degree circular
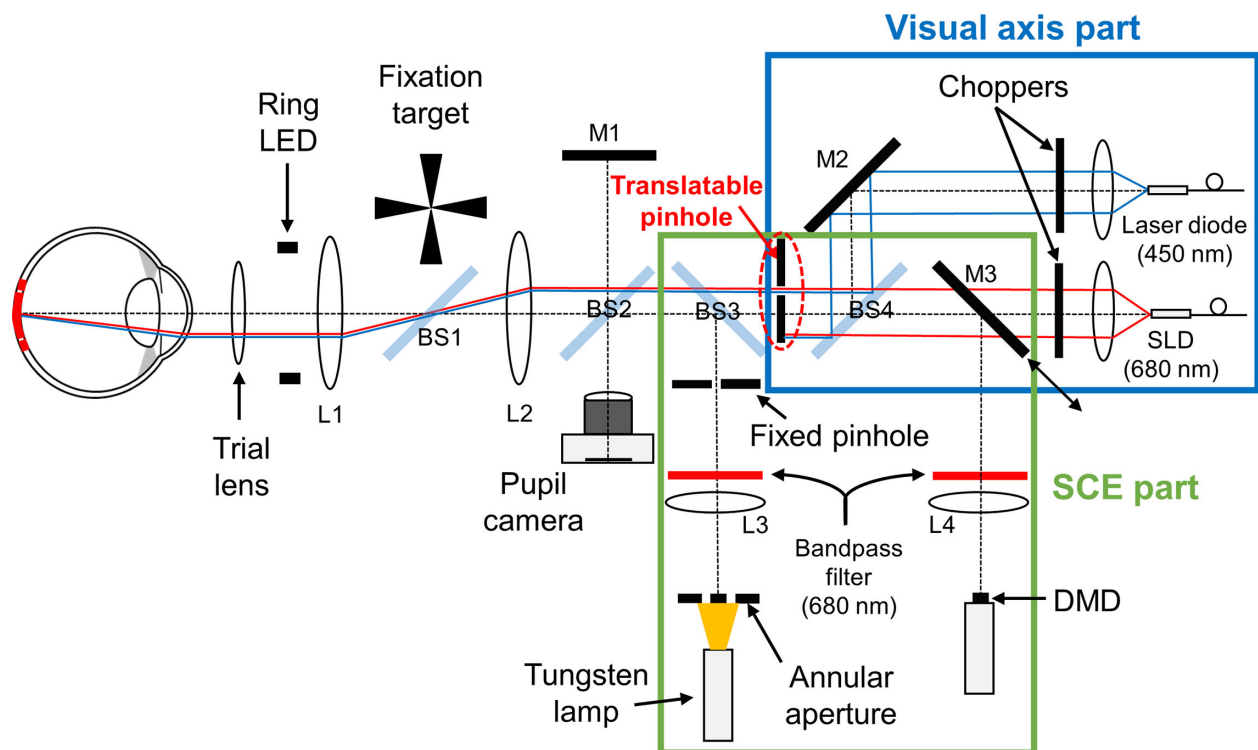
FIGURE 1. Schematic of the visual axis and Stiles–Crawford effect (SCE) testing system. LED, light-emitting diode; SLD, super-luminescent diode; DMD, digital micromirror device; L, lens; BS, pellicle beam splitter; M, mirror.
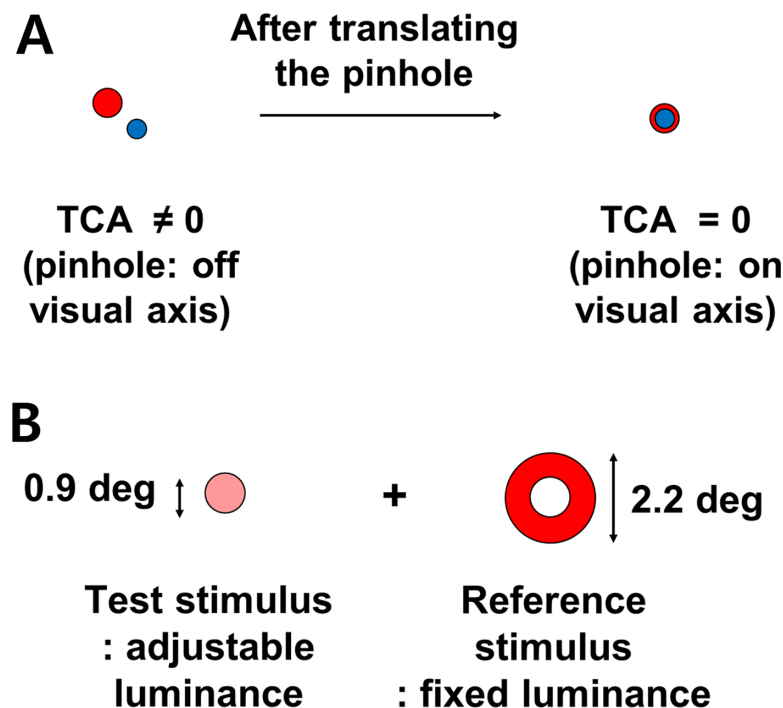
FIGURE 2. Schematic diagrams of what the participant would see (**A**) during the visual axis measurement and (**B**) during the Stiles–Crawford effect measurement. Note that the *red* stimulus is comparably larger than the *blue* stimulus because of the wavelength effect on the Airy disk size. TCA, transverse chromatic aberration.

central test stimulus. The other source, the tungsten lamp, was relayed by lens L3, a fixed pinhole (600 µm diameter), and a pellicle beam splitter (BS3). This source provided the participant with a 0.9 degree (inner)/2.2 degree (outer) ring-shaped reference stimulus, defined by the annular aperture. Another identical bandpass filter was applied in front of L3.

Participants

In this cohort study, we obtained data for 12 eyes from 6 healthy individuals (4 men and 2 women). Participants with astigmatism larger than 1.5 diopters (D) or ocular abnormalities that could affect the result, such as color blindness, were excluded. Pupils were dilated with each drop of 1% tropicamide and 2.5% phenylephrine before measurements.

Measurement Procedure

Visual Axis. The measurement procedure launched for the alignment of the pupil of the eye with the optical axis of the apparatus used real-time images supported by the pupil camera. The participant would see two separate blue and red spots, owing to the eye's transverse chromatic aberration (Fig. 2A). Then, the participant was asked to adjust the x and y position of the motorized translatable pinhole until the colored dots were superimposed. This position is achieved only when the translatable pinhole is on the visual axis. Otherwise, some misalignment is perceived because of the induced TCA. Once both dots were aligned, the participant should fixate steadily on the superimposed dots. Concurrently, the examiner saved the pupil image, including the visual axis position. This procedure was repeated
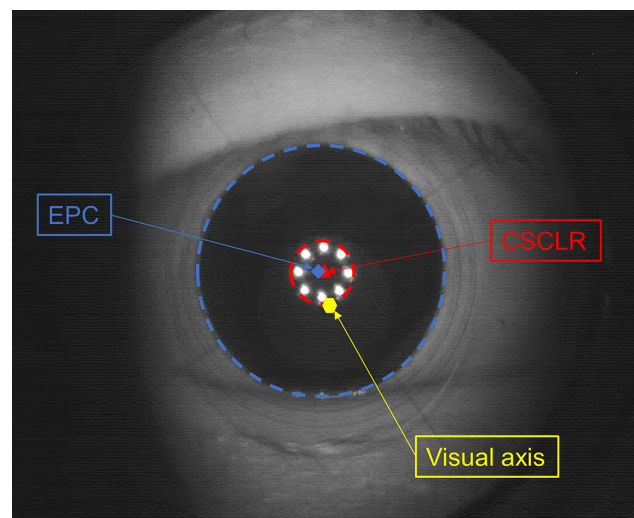
FIGURE 3. An exemplary pupil camera image from one participant's eye. The image was analyzed to obtain the position of the visual axis (*yellow hexagon*) and coaxially sighted corneal light reflex (CSCLR, *red triangle*), with respect to the entrance pupil center (EPC, *blue diamond*).

five times for each eye, and the data were averaged. The image recorded was later analyzed manually using ImageJ (National Institutes of Health) to obtain the positions of the EPC, visual axis, and CSCLR (defined by the centroid of the first Purkinje image from ring LEDs). Figure 3 demonstrates an exemplary pupil image to assess the visual axis position from the EPC and the CSCLR for comparison.

Stiles–Crawford Effect. To measure directional sensitivity, a two-channel Maxwellian-view optical system was built to produce images of the two stimuli in the plane of the participant's retina (see Fig. 1). The DMD was programmed using MATLAB (Mathworks) to control the brightness of the test stimulus. The luminance of the test stimulus was continuously adjusted by the participant over a 2-log-unit range. The steady surrounding reference stimulus provided fixed luminance (0.2 cd/m^2). Nineteen pupillary entry points of the test stimulus were sampled at 1 mm steps over a 4 mm diameter pupillary region with respect to the EPC in a hexagonal sampling configuration. Because the initial luminance of the test stimulus was randomly assigned at each pupil-entry location, the participant needed to increase or decrease the luminance of the test stimulus until it completely matched the surrounding reference stimulus luminance (see Fig. 2B).

Data Analysis

Dedicated routines in MATLAB were used to estimate the sensitivity at each pupil entry and to fit the relative luminous sensitivity (defined as the ratio of the luminance of a fixed reference entering the center of the pupil to the luminance of a displaced test beam) to bidirectional Gaussian profiles for average sensitivity data across three consecutive measurements. The following function was used for a least-squares fit program to fit the sensitivity as a function of the pupil entry position:

$$\eta\left(x, y\right)$$
$$= \eta_{max} 10^{-\rho_x\left((x-x_0)\cos\theta - (y-y_0)\sin\theta\right)^2 - \rho_y\left((x-x_0)\sin\theta + (y-y_0)\cos\theta\right)^2}$$

where η_{max} is the sensitivity at the peak, ρ_x and ρ_y are the shape factors, x_o and y_o are the pupillary coordinates of the peak, and θ is the rotation angle (positive if anti-clockwise in right eyes and negative in left eyes) of the rotated x'–y' coordinates of the Gaussian fit with respect to the x-y coordinates of the participant's pupil.

Statistical Analysis

Mirror symmetry analyses between pairs of continuous variables were performed using bivariate correlation analysis (2-tailed) once normality was verified using the Kolmogorov–Smirnov test. Correlation analyses between pairs of continuous variables were performed using generalized estimating equations,[26] to address the possibility of correlation between eyes. The goodness of fit was estimated with the marginal R^2 proposed by Zheng[27] was used. Interclass correlation coefficients (ICCs) were determined to evaluate the agreement between the visual axis and other positions. Statistical significance was set at a P value < 0.05. All analyses were performed using Statistical Package for the Social Sciences software (version 25.0; IBM Corp.) and Rstudio software (Rstudio Team).

RESULTS

The participants' mean age was 29.3 ± 5.9 years (range = 21–41 years). The average refraction of the population was myopic, with a mean spherical equivalent of −3.9 ± 2.8 D (range = −8.5 to +0.5 D). Ophthalmic trial lenses or contact lenses were used to correct the refractive error. The magnification factor induced by an ophthalmic trial lens was corrected after data acquisition.

Figures 4A and 4B show the distribution of the visual axis and SCE peak positions in the pupil plane for participants' right and left eyes. Ten participants (20 eyes) had their visual axes and SCE peaks within 1 mm of one eye from the EPC, demonstrating intersubject variability. On average, the visual axis was inferonasal to the EPC (x = 0.24 ± 0.35 mm, y = −0.16 ± 0.34 mm). The SCE peak was also inferonasal to
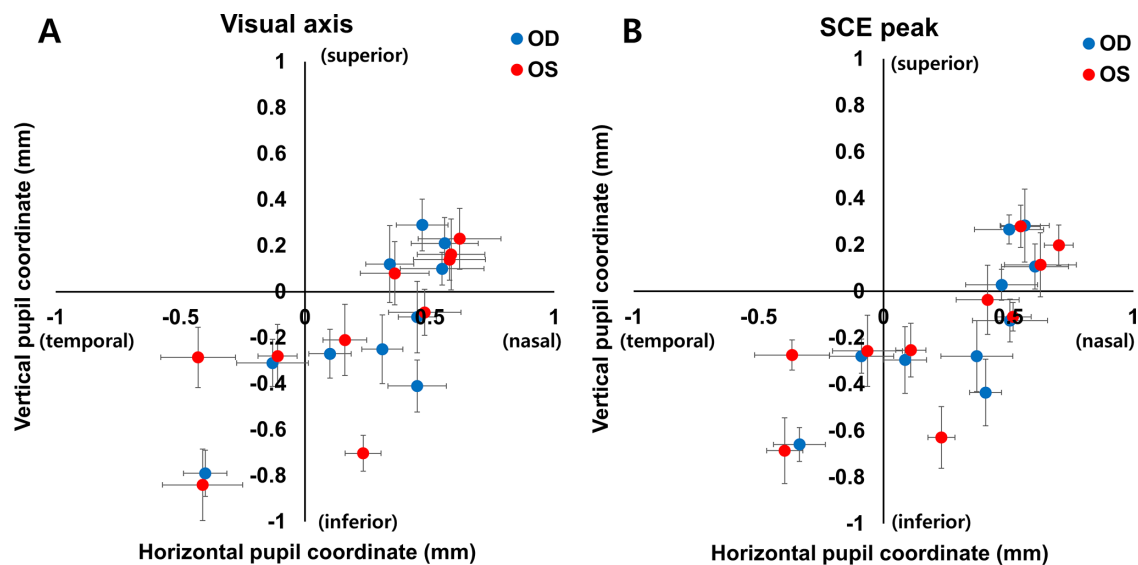
FIGURE 4. Distribution of the visual axes and Stiles–Crawford effect (SCE) peaks in both eyes of 10 participants. Coordinates of the visual axis and SCE peak were defined in reference to the entrance pupil center. These plots represent a comparison of the estimates of the visual axis and SCE peak position between the x (horizontal direction, temporal-nasal) and y (vertical direction, inferior-superior). Each data point was averaged over the five runs. The positive x and y axes represent nasal and superior pupils, respectively. *Blue circles* represent right eyes and *red circles* represent left eyes. The visual axis and SCE peak positions show remarkable intersubject variability. Error bars represent standard deviations of repeated measurements.
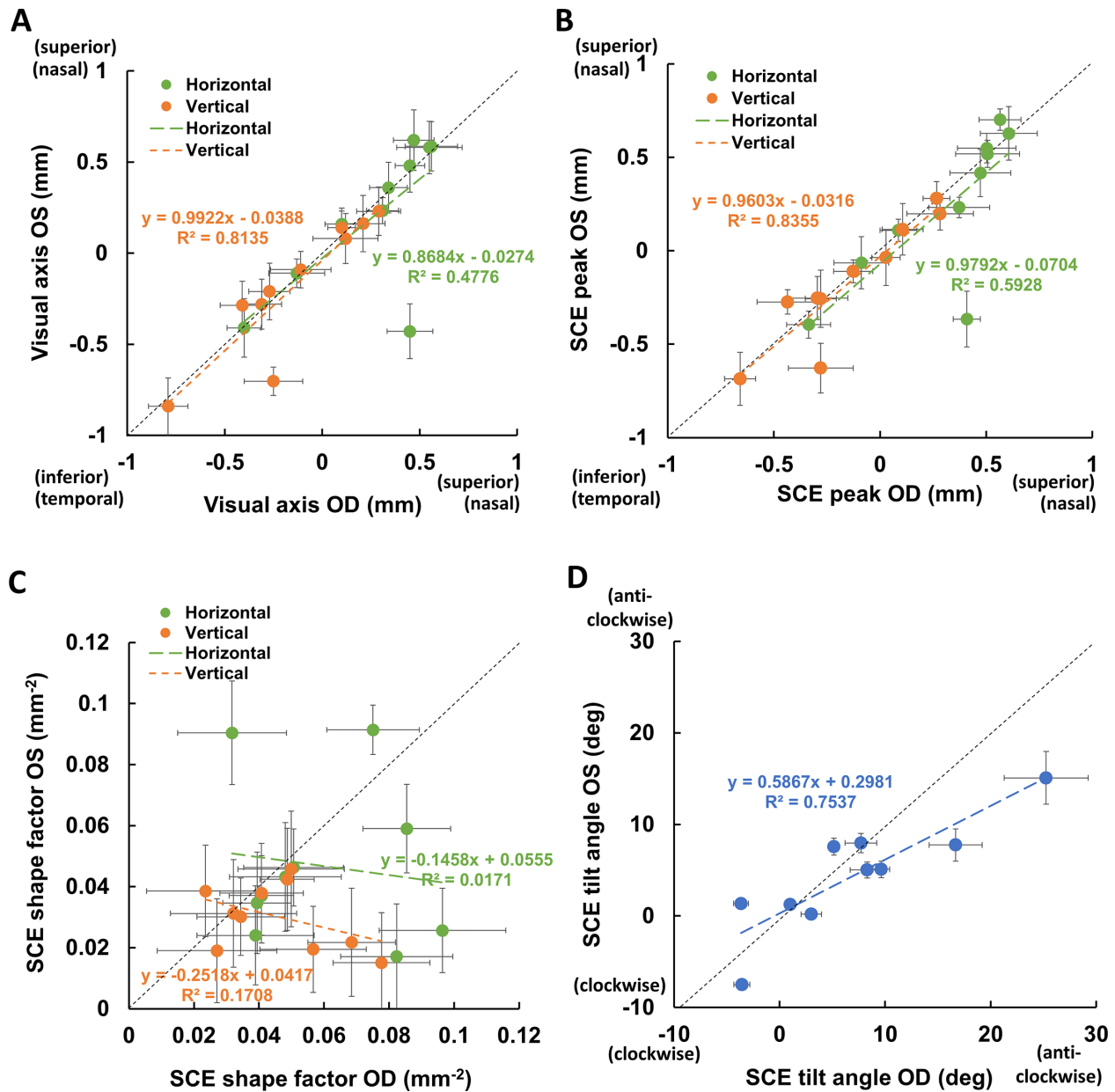
FIGURE 5. Mirror symmetry of each parameter related to the visual axis and cone photoreceptor directionality. (**A**) Visual axis coordinate, (**B**) Stiles–Crawford effect (SCE) peak coordinate, (**C**) SCE shape factor, and (**D**) SCE tilt angle. *Green symbols* represent horizontal coordinates or values. *Orange symbols* represent vertical coordinates or values. Coordinates of the visual axis and SCE peak were defined in reference to the entrance pupil center. Negative coordinates represent temporal and inferior pupil locations, and positive coordinates represent nasal and superior pupil locations. The *thin dashed lines* represent the mirror symmetry lines. Error bars represent standard deviations of repeated measurements. OD, right eye; OS, left eye.

the EPC (x = 0.27 ± 0.35 mm, y = −0.15 ± 0.31 mm). The visual axes and SCE peak positions were located in three quadrants only, and no data points were measured in the superotemporal region.

Figures 5A, 5B, and 5C show the mirror symmetry of the visual axis and parameters related to the SCE in the horizontal and vertical meridians. In Figure 5A, the correlations of the visual axis for both horizontal coordinates ($R^2 = 0.48$, $P = 0.027$) and vertical coordinates ($R^2 = 0.81$, $P < 0.001$) were significant. In Figure 5B, the correlations of the SCE peak position for both horizontal coordinates ($R^2 = 0.84$, $P < 0.001$) and vertical coordinates ($R^2 = 0.59$, $P = 0.009$) were

also significant. Other parameters that described the Gaussian distribution of light guided by the cone photoreceptors were shape factor ρ and tilt angle θ. Figure 5C shows the P values for the right versus left eyes. There was no statistically significant mirror symmetry for the shape factors in the horizontal and vertical meridians ($P = 0.72$ and 0.24, respectively). Figure 5D shows the θ values for the right versus the left eyes. The correlation between the tilt angles was statistically significant ($R^2 = 0.75$, $P = 0.001$), indicating mirror symmetry for the tilt angles.

Figures 6A and 6B show the visual axis and SCE peak coordinates, respectively, for eyes with different refractive
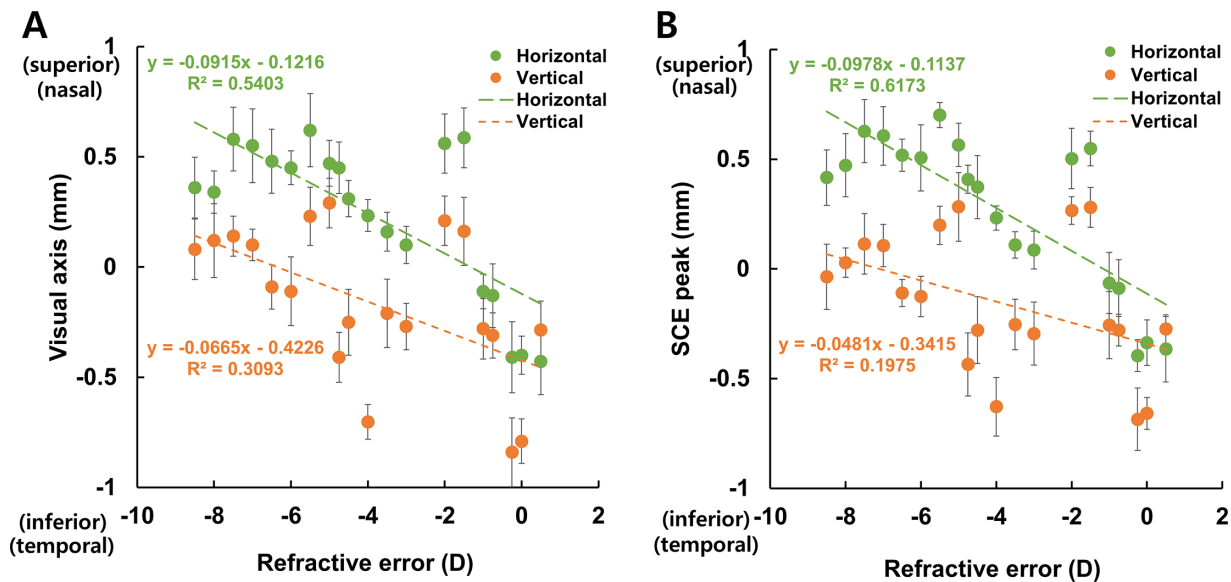
FIGURE 6. Visual axis (**A**) and Stiles–Crawford effect (SCE) peak (**B**) coordinates in 20 eyes of different refractive errors. Coordinates of the visual axis and SCE peak were defined in reference to the entrance pupil center. The visual axis and SCE peak coordinates show statistically significant correlations with the refractive errors only in the horizontal meridian. Error bars represent standard deviations of repeated measurements. D, diopters.
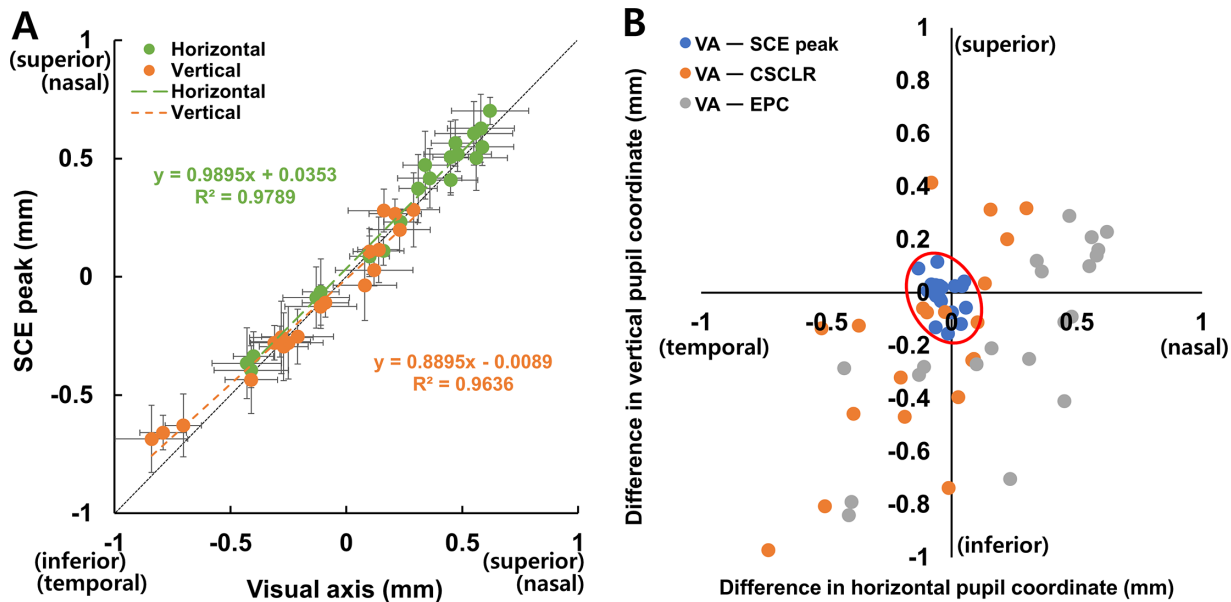

FIGURE 7. (**A**) Correlation between coordinates of the visual axis and Stiles–Crawford effect (SCE) peak. Coordinates of the visual axis and SCE peak were defined in reference to the entrance pupil center. The visual axis and SCE peak positions show a significant linear correlation in both meridians. The *thin solid line* represents the equality line. Error bars represent standard deviations of repeated measurements. (**B**) Visual axis (VA) positions compared with those of Stiles–Crawford effect (SCE) peak, coaxially sighted corneal light reflex (CSCLR), and entrance pupil center (EPC). The *red circle* shows the 95% confidence interval of the VA positions compared to that of the SCE peak (i.e. no significant difference was within the outline).

errors. The correlations of the visual axis coordinates ($R^2 = 0.54$, $P = 0.030$) and SCE peak coordinates ($R^2 = 0.62$, $P = 0.023$) for the horizontal meridian were statistically significant, indicating that the myopic eyes tended to locate the visual axis and SCE peak locations nasally. There were no statistically significant trends for the visual axis or SCE peak coordinates in the vertical meridians ($P = 0.488$ and 0.434, respectively).

Figure 7A shows the correlation between the coordinates of the visual axis and the SCE peak for both eyes. The visual axis and SCE peak positions showed a statistically significant linear correlation (horizontal coordinates: $R^2 = 0.98$, $P = 0.012$; vertical coordinates: $R^2 = 0.96$, $P = 0.023$). Figure 7B shows the distribution of the visual axis relative to the SCE peak, CSCLR, and EPC. The visual axis and SCE peak positions demonstrated no significant difference but good

agreement (ICC = 0.988), whereas the CSCLR showed significant but poor agreement with the visual axis (ICC = 0.467). Because the visual axis position was measured with respect to the EPC, statistical analysis was not possible between the visual axis and EPC. However, the distribution of the EPC, with respect to the visual axis, could be compared to those of the SCE peak and CSCLR.

DISCUSSION

We developed an optical system to subjectively determine the position of the visual axis and SCE peak on the pupil plane in healthy participants. Our results showed that the pupillary locations of the visual axis were remarkably well correlated with the SCE peak compared to the CSCLR and EPC. We also found a significant mirror symmetry of the visual axes and SCE peak positions. These findings suggest that the functional orientation of cone photoreceptors is associated with the visual axis along which the transverse chromatic aberration is zero.

Because the fovea lies off the optical axis of the eye and the lens and cornea are slightly tilted and decentered to each other, the human eye is not a rotationally symmetric or centered optical system.[28] These multiple misaligned refractive surfaces cause challenges in the optical characterization of the eye and clinical decisions for centration. Recently, researchers have been using the subject-fixated CSCLR as the clinical reference for centration.[3] It is commonly assumed that the CSCLR is close to the intersection of the visual axis on the pupil plane.[3] However, our study found a significant discrepancy between the CSCLR and the visual axis. Manzanera et al.[29] already reported that 27% of healthy eyes showed a statistically significant distance between the CSCLR and visual axis, and in 5% of cases, the distance was >0.4 mm. Moreover, their simulation study demonstrated that the linear addition of the effects of the crystalline lens decentration, tilt, and thickness could account for this discrepancy. The distance between the CSCLR and the visual axis may be explained by the difference between the center of the anterior corneal curvature (related to the CSCLR) and the anterior nodal point (related to the visual axis).

In addition, another discrepancy exists among the currently available devices for the measurement of angle κ. Undoubtedly, angle κ plays a critical role in laser corneal refractive surgery[1,30] and the implantation of multifocal intraocular lenses.[31,32] The definition of angle κ in the literature is conflicting because the same angle (angle κ) has been used to specify two different angles.[3] Although angle κ has been commonly accepted, angle λ is distinctly defined as the angle between the pupillary axis and LOS.[3,31] Angle κ has been used interchangeably with angle λ basis of the assumption that both angles are similar when the fixation point is far away from the pupil plane.[3] However, clinicians should be careful because the visual axis differs from the LOS and the CSCLR. For example, Pentacam reported the distance from the CSCLR to the EPC only,[33] and not from the visual axis.

In our study, the coordinates of the visual axis on the pupil plane clearly showed intersubject variability. This intersubject variability was consistent with the findings of previous studies.[34,35] Theoretical eye models estimated that the vertical component might be approximately half of the horizontal component in the visual axis–EPC difference.[36] Those estimations were based on the foveal displacement relative to the optical axis. Variability in the visual axis locations from the EPC cannot be explained only by angle α, the angle between the visual axis and optical axis, but may also be interpreted by misalignment of the cornea, crystalline lens, and iris. Individual differences in the refractive indices, especially in crystalline lenses with a gradient index, may also play a role in the diversity of the visual axis position.

The coordinates of the SCE peak also varied widely among participants. Previous studies using psychophysical[11,25,37] and reflectometric measurements[19,37–40] demonstrated large intersubject variability in cone orientation. Phototropism has been proposed as a potential mechanism underlying cone orientation.[19–24] Kono et al.[24] found minor nasal shifts of the SCE peak after 8 days of dark patching, whereas a substantial temporal re-adjustment after 3 day's recovery, supporting the phototropic mechanism in normal eyes. Applegate and Bonds[22] reported the SCE peak shift toward an artificial pupil after wearing a contact lens with the 2-mm centered artificial pupil in a nasally displaced pupil after trauma. Smallman et al.[23] presented the SCE peak shift toward the pupil center after congenital cataract extraction. However, what drives the cone photoreceptors to point toward the given pupil position remains unclear. Marcos and Burns[19] proposed that optical aberrations and cone directionality may interact, so the pupil's best optical area corresponds to the area of maximum transmittance. They also reported that cone photoreceptors did not point toward optically degraded pupil positions; maximal cone directionality coincides with the pupillary region of the best optical quality for some eyes only.[19] Our results implied that the SCE peak might lie adjacent to the visual axis. The potential visual advantage of this finding could be the maximization of polychromatic visual quality by minimizing TCA. The cone photoreceptors cannot adjust their orientation quickly as to the dynamics of vision (e.g. eye movement), and the optimal direction of alignment may be different in three types of cones.[41] The best strategy may be achromatizing the pupil position corresponding to the visual axis. However, this hypothesis must be tested.

The mirror symmetry between the two eyes was noticeable on the visual axis and the SCE peak position. First, the mirror symmetry of the visual axis position may indicate anatomical symmetry in terms of the shape and layout of each ocular optical element, which may also explain the mirror symmetry of the SCE tilt angle. Furthermore, the mirror symmetry in the SCE peak may support the potential systematic mechanism of the cone orientation. Assuming the active phototropic capability of cone photoreceptors, they may point toward the second nodal point of the eye, which is close to the plane of the pupil,[42,43] and also toward one part of the visual axis. Based on the definition of the nodal point, this may produce angular linearity for rays transmitted through the pupil and toward the curved retina[42] and may optimize the capture efficiency of the cone photoreceptors for light with minimal TCA. Interestingly, the shape factor ρ did not show direct symmetry, which conflicted with a previous finding.[19] This implies that the factors regulating the distribution widths of the cone directionality may be between the two eyes due to differences in cone spacing or aperture size distribution and the structural features of the cones.[37,44]

In our study, 9 participants had 17 myopic eyes and showed a tendency for nasal bias in cone photoreceptor alignment. This finding is somewhat consistent with previous studies,[25,45–48] which reported nasal bias in myopic

individuals. The anatomic sections of myopic eyes indicate a slope in the sclera (i.e. the temporal retina is anterior to the nasal retina). Westheimer[48] suggested that the fovea has a sloping shape factor that makes the foveal cone photoreceptors point toward the nasal pupillary area. Furthermore, the tractional force on the retina has been suggested to affect cone photoreceptor alignment.[20] Choi et al.[45] hypothesized a potential scenario associated with an extension of the vitreous chamber depth. Specifically, they speculated that when the eye elongates axially in myopic eyes, the anterior vitreomacular traction might apply a pulling force to the nasal retina between the optic nerve head and fovea. This force originating near the optic disc's temporal rim may drag the cone photoreceptors nasally.

On the other hand, the visual axis also demonstrated a nasally biased position. A recent study showed that crystalline lenses were tilted outward, and the tilt magnitude tended to be lower in myopic eyes than in non-myopic eyes.[49] If the crystalline lenses are tilted inward in myopic eyes, the first nodal point is shifted nasally so that it may affect the visual axis position on the pupil plane. Further studies are required to test these hypotheses.

A major limitation of this study was the subjective nature of psychophysical measurements, where the retina operated as a detector after a single pass of light through the ocular media. The measurement errors in terms of standard deviations in our repeated measurements might have occurred because of these subjective characteristics. Although SCE has been commonly studied by psychophysical methods, it demands a high level of concentration among the participants and involves lengthy sessions, making it difficult to use in a clinical setting.[25] Instead, objective methods that use the reflectometric technique[38,39] can be applied, and are faster and more patient-friendly than the psychophysical measurements. We could not use the objective reflectometric method for the SCE measurement because of the absence of a current method to measure the visual axis objectively to avoid a mismatch in measurements between the visual axis and SCE. Recent studies have proposed a technique to measure human ocular TCA by adopting an adaptive optics scanning laser ophthalmoscope with a wide object instead of a point source.[50,51] It may be plausible to measure the visual axis objectively using this approach by scanning for TCA on the pupil plane.

The SCE was measured at a single wavelength (680 nm); therefore, the potential influence of wavelength on the SCE could not be ruled out. The shape factor ρ tends to increase with longer wavelengths,[11,52–55] and the SCE peak position shows relatively small but opposite horizontal shifts between 570 nm and 670 nm in 2 participants.[55] Further studies are warranted to determine the cause of these wavelength-dependent changes in the SCE.

Our experimental protocol could not elucidate any visual benefit of choosing the visual axis as a centration reference compared to the CSCLR or EPC. A direct comparative study of the visual performance of each reference would help evaluate the benefit.[56] Moreover, to clarify the potential interaction between retinal image quality and cone alignment, highly aberrated eyes, such as keratoconus, would be a promising model to test this hypothesis. Additionally, whether there is a closed-loop mechanism (feedback between polychromatic retinal image quality and cone alignment) should be clarified to rationalize the cone directionality toward the visual axis. Furthermore, it is important to study the correlation between the visual axis and cone direc-

tionality in abnormal conditions such as eccentric fixation or age-related macular degeneration with a preferred retinal locus.

In summary, a significant positional correlation between the visual axis and cone directionality was observed in the present study. The mirror symmetry and refractive error correlation of the visual axis and cone directionality may also support this positional interconnection, indicating the potential role of the visual axis as an optical cue mediating cone orientation. These findings may provide a clearer understanding of the clinical implications of the visual axis and further research topics, including anatomic and/or optical factors for cone photoreceptor alignment.

Disclosure: **S.P. Bang**, None; **J. Lyu**, None; **C.J. Ng**, None; **G. Yoon**, None

References

1. Arba Mosquera S, Verma S, McAlinden C. Centration axis in refractive surgery. *Eye Vis (Lond)*. 2015;2:4.

2. Pande M, Hillman JS. Optical zone centration in keratorefractive surgery. Entrance pupil center, visual axis, coaxially sighted corneal reflex, or geometric corneal center? *Ophthalmology*. 1993;100:1230–1237.

3. Chang DH, GO 4th Waring. The subject-fixated coaxially sighted corneal light reflex: a clinical marker for centration of refractive treatments and devices. *Am J Ophthalmol*. 2014;158:863–874.

4. Okamoto S, Kimura K, Funakura M, Ikeda N, Hiramatsu H, Bains HS. Comparison of myopic LASIK centered on the coaxially sighted corneal light reflex or line of sight. *J Refract Surg*. 2009;25:S944–S950.

5. Okamoto S, Kimura K, Funakura M, Ikeda N, Hiramatsu H, Bains HS. Comparison of wavefront-guided aspheric laser in situ keratomileusis for myopia: coaxially sighted corneal-light-reflex versus line-of-sight centration. *J Cataract Refract Surg*. 2011;37:1951–1960.

6. Arbelaez MC, Vidal C, Arba-Mosquera S. Clinical outcomes of corneal vertex versus central pupil references with aberration-free ablation strategies and LASIK. *Invest Ophthalmol Vis Sci*. 2008;49:5287–5294.

7. Chang JS, Law AK, Ng JC, Chan VK. Comparison of refractive and visual outcomes with centration points 80% and 100% from pupil center toward the coaxially sighted corneal light reflex. *J Cataract Refract Surg*. 2016;42:412–419.

8. Guyton DL. More on optical zone centration. *Ophthalmology*. 1994;101:793–794.

9. Ivanoff A. Optique Physiologique - Sur Une Methode De Mesure Des Aberrations Chromatiques Et Spheriques De Loeil En Lumiere Dirigee. *Cr Hebd Acad Sci*. 1946;223:170–172.

10. Thibos LN, Bradley A, Still DL, Zhang X, Howarth PA. Theory and measurement of ocular chromatic aberration. *Vision Res*. 1990;30:33–49.

11. Stiles WS, Crawford BH. The luminous efficiency of rays entering the eye pupil at different points. *Proc R Soc Lond B Biol Sci*. 1933;112:428–450.

12. Westheimer G. Directional sensitivity of the retina: 75 years of Stiles-Crawford effect. *Proc R Soc Lond B Biol Sci*. 2008;275:2777–2786.

13. Westheimer G. Dependence of the magnitude of the Stiles-Crawford effect on retinal location. *J Physiol*. 1967;192:309–315.

14. Enoch JM, Laties AM. An analysis of retinal receptor orientation. II. Predictions for psychophysical tests. *Invest Ophthalmol*. 1971;10:959–970.

15. Vohnsen B, Iglesias I, Artal P. Guided light and diffraction model of human-eye photoreceptors. *J Opt Soc Am A Opt Image Sci Vis*. 2005;22:2318–2328.

16. Vohnsen B, Carmichael A, Sharmin N, Qaysi S, Valente D. Volumetric integration model of the Stiles-Crawford effect of the first kind and its experimental verification. *J Vis*. 2017;17:18.

17. Vohnsen B. Directional sensitivity of the retina: A layered scattering model of outer-segment photoreceptor pigments. *Biomed Opt Express*. 2014;5:1569–1587.

18. Vohnsen B. Geometrical scaling of the developing eye and photoreceptors and a possible relation to emmetropization and myopia. *Vis Res*. 2021;189:46–53.

19. Marcos S, Burns SA. On the symmetry between eyes of wavefront aberration and cone directionality. *Vis Res*. 2000;40:2437–2447.

20. Enoch JM. Marked accommodation, retinal stretch, monocular space perception and retinal receptor orientation. *Am J Optom Physiol Opt*. 1975;52:376–392.

21. Bonds AB, MacLeod DI. A displaced Stiles-Crawford effect associated with an eccentric pupil. *Invest Ophthalmol Vis Sci*. 1978;17:754–761.

22. Applegate RA, Bonds AB. Induced movement of receptor alignment toward a new pupillary aperture. *Invest Ophthalmol Vis Sci*. 1981;21:869–872.

23. Smallman HS, MacLeod DI, Doyle P. Vision. Realignment of cones after cataract removal. *Nature*. 2001;412:604–605.

24. Kono M, Enoch JM, Strada E, et al. Stiles-Crawford effect of the first kind: assessment of photoreceptor alignments following dark patching. *Vis Res*. 2001;41:103–118.

25. Applegate RA, Lakshminarayanan V. Parametric representation of Stiles-Crawford functions: normal variation of peak location and directionality. *J Opt Soc Am A*. 1993;10:1611–1623.

26. Murdoch IE, Morris SS, Cousens SN. People and eyes: statistical approaches in ophthalmology. *Br J Ophthalmol*. 1998;82:971–973.

27. Zheng B. Summarizing the goodness of fit of generalized linear models for longitudinal data. *Stat Med* .2000;19:1265–1275.

28. Uozato H, Guyton DL. Centering corneal surgical procedures. *Am J Ophthalmol*. 1987;103:264–275.

29. Manzanera S, Prieto PM, Benito A, Tabernero J, Artal P. Location of achromatizing pupil position and first Purkinje reflection in a normal population. *Invest Ophthalmol Vis Sci*. 2015;56:962–966.

30. Shao T, Wang Y, Ng ALK, et al. The Effect of Intraoperative Angle Kappa Adjustment on Higher-Order Aberrations Before and After Small Incision Lenticule Extraction. *Cornea*. 2020;39:609–614.

31. Park CY, Oh SY, Chuck RS. Measurement of angle kappa and centration in refractive surgery. *Curr Opin Ophthalmol*. 2012;23:269–275.

32. Fu Y, Kou J, Chen D, et al. Influence of angle kappa and angle alpha on visual quality after implantation of multifocal intraocular lenses. *J Cataract Refract Surg*. 2019;45:1258–1264.

33. Rodriguez-Vallejo M, Pinero DP, Fernandez J. Avoiding misinterpretations of Kappa angle for clinical research studies with Pentacam. *J Optom*. 2019;12:71–73.

34. Rynders M, Lidkea B, Chisholm W, Thibos LN. Statistical distribution of foveal transverse chromatic aberration, pupil centration, and angle psi in a population of young adult eyes. *J Opt Soc Am A Opt Image Sci Vis*. 1995;12:2348–2357.

35. Simonet P, Campbell MC. The optical transverse chromatic aberration on the fovea of the human eye. *Vis Res*. 1990;30:187–206.

36. Thibos LN. Calculation of the influence of lateral chromatic aberration on image quality across the visual field. *J Opt Soc Am A*. 1987;4:1673–1680.

37. Morris HJ, Blanco L, Codona JL, Li SL, Choi SS, Doble N. Directionality of individual cone photoreceptors in the parafoveal region. *Vis Res*. 2015;117:67–80.

38. Gorrand JM, Delori F. A reflectometric technique for assessing photoreceptor alignment. *Vis Res*. 1995;35:999–1010.

39. Burns SA, Wu S, Delori F, Elsner AE. Direct measurement of human-cone-photoreceptor alignment. *J Opt Soc Am A Opt Image Sci Vis*. 1995;12:2329–2338.

40. Roorda A, Williams DR. Optical fiber properties of individual human cones. *J Vis*. 2002;2:404–412.

41. Eckmiller MS. Defective cone photoreceptor cytoskeleton, alignment, feedback, and energetics can lead to energy depletion in macular degeneration. *Prog Retin Eye Res*. 2004;23:495–522.

42. Simpson MJ. Nodal points and the eye. *Appl Opt*. 2022;61:2797–2804.

43. Harris WF. Nodes and nodal points and lines in eyes and other optical systems. *Ophthalmic Physiol Opt*. 2010;30:24–42.

44. Marcos S, Burns SA, He JC. Model for cone directionality reflectometric measurements based on scattering. *J Opt Soc Am A Opt Image Sci Vis*. 1998;15:2012–2022.

45. Choi SS, Garner LF, Enoch JM. The relationship between the Stiles-Crawford effect of the first kind (SCE-I) and myopia. *Ophthalmic Physiol Opt*. 2003;23:465–472.

46. Singh N, Atchison DA, Kasthurirangan S, Guo H. Influences of accommodation and myopia on the foveal Stiles–Crawford effect. *J Modern Optics*. 2009;56:2217–2230.

47. Carmichael Martins A, Vohnsen B. Analysing the impact of myopia on the Stiles-Crawford effect of the first kind using a digital micromirror device. *Ophthalmic Physiol Opt*. 2018;38:273–280.

48. Westheimer G. Entoptic visualization of Stiles-Crawford effect. An indicator of eyeball shape. *Arch Ophthalmol*. 1968;79:584–588.

49. Lu Q, He W, Qian D, Lu Y, Zhu X. Measurement of crystalline lens tilt in high myopic eyes before cataract surgery using swept-source optical coherence tomography. *Eye Vis (Lond)*. 2020;7:14.

50. Harmening WM, Tiruveedhula P, Roorda A, Sincich LC. Measurement and correction of transverse chromatic offsets for multi-wavelength retinal microscopy in the living eye. *Biomed Opt Express*. 2012;3:2066–2077.

51. Winter S, Sabesan R, Tiruveedhula P, et al. Transverse chromatic aberration across the visual field of the human eye. *J Vis*. 2016;16:9.

52. Enoch JM, Stiles WS. The Colour Change of Monochromatic Light with Retinal Angle of Incidence. *Opt Acta: International Journal of Optics*. 1961;8:329–358.

53. Alpern M, Kitahara K. The directional sensitivities of the Stiles' colour mechanisms. *J Physiol*. 1983;338:627–649.

54. Lochocki B, Rativa D, Vohnsen B. Spatial and spectral characterisation of the first and second Stiles–Crawford effects using tuneable liquid-crystal filters. *J Modern Optics*. 2011;58:1817–1825.

55. Lochocki B, Vohnsen B. Defocus-corrected analysis of the foveal Stiles–Crawford effect of the first kind across the visible spectrum. *J Optics*. 2013;15:125301.

56. Atchison DA, Marcos S, Scott DH. The influence of the Stiles-Crawford peak location on visual performance. *Vis Res*. 2003;43:659–668.